

Spectral Observations of Optical Emissions Associated with Terrestrial Gamma-Ray Flashes

Matthias Heumesser¹, Olivier Chanrion¹, Torsten Neubert¹, Hugh Christian²,
Christoph Köhn¹, Krystallia Dimitriadou¹, Francisco J. Gordillo-Vazquez³,
Alejandro Luque³, Francisco Javier Pérez-Invernón^{3,4}, Richard J. Blakeslee⁵,
Andrey Mezentsev⁶, Nikolai Østgaard⁶ and Victor Reglero⁷.

¹National Space Institute, Technical University of Denmark (DTU Space), Denmark

²Earth System Science Center, University of Alabama in Huntsville, Alabama, USA

³Instituto de Astrofísica de Andalucía (IAA, CSIC), Granada, Spain

⁴Institut für Physik der Atmosphäre, Deutsches Zentrum für Luft- und Raumfahrt, Wessling, Germany

⁵NASA Marshall Space Flight Center, Huntsville, Alabama, USA

⁶Birkeland Centre for Space Science, University of Bergen, Bergen, Norway

⁷Image Processing Laboratory, University of Valencia, Valencia, Spain

Key Points:

- We present the first statistical analysis of emissions at 180-230 nm, 337 nm and 777 nm coincident with TGFs as measured by a single platform
- 90% of TGFs occur at the onset of large-amplitude optical pulses and thus support the streamer-leader model for TGF generation
- The sources of the emissions are estimated to be 1-5 km below the cloud tops

Index Terms:

ASIM, ISS, Optical Radiation, TGF, Streamer, Leader

Corresponding author: Matthias Heumesser, heumat@space.dtu.dk

22 **Abstract**

23 The Atmosphere-Space Interactions Monitor measures Terrestrial Gamma-Ray Flashes
24 (TGFs) simultaneously with optical emissions from associated lightning activity. We an-
25 alyzed optical measurements at 180-230 nm, 337 nm and 777.4 nm related to 69 TGFs
26 observed between June 2018 and October 2019. All TGFs are associated with optical
27 emissions with 90% at the onset of a large optical pulse, suggesting that they are con-
28 nected with the initiation of current surges. A simple model of photon delay induced by
29 cloud scattering suggests that the sources of the optical pulses are from 0.7 ms before
30 to 4.4 ms after the TGFs, with a median of $-10 \pm 80 \mu\text{s}$, and 1-5 km below the cloud top.
31 The pulses have rise times comparable to lightning without identified TGFs, while the
32 FWHM is twice as long. Pulse amplitudes at 337 nm are ~ 3 times larger than at 777.4
33 nm. The results support the leader-streamer mechanism for TGF generation.

34 **Plain Language Summary**

35 Terrestrial Gamma-Ray Flashes (TGFs) are short bursts of high-energy radiation
36 produced in thunderstorms, first observed from astrophysical spacecraft during the 1990s.
37 This study characterizes optical emissions from lightning associated with these flashes
38 in multiple wavelengths to help finding their production mechanism. The data are col-
39 lected by space based instruments aboard the International Space Station as it passes
40 over the major thunderstorm regions of the Earth. We find that TGFs are associated
41 with propagation of intra-cloud lightning in the upper cloud levels. With the help of a
42 model of light propagation through a cloud, we estimate the source of the respective op-
43 tical emissions to be 1-5 km below the cloud tops. By investigating TGFs and their con-
44 nection to lightning, we can understand the energy- and timescales of lightning better,
45 eventually leading to a better understanding of cloud physics and thunderstorms in gen-
46 eral.

47 **1 Introduction**

48 Terrestrial Gamma-Ray Flashes (TGFs) are bursts of X- and gamma-rays from thun-
 49 derstorms (Fishman et al., 1994). They are bremsstrahlung from relativistic runaway elec-
 50 trons, powered by the electric fields within the thunderstorm clouds (Wilson, 1925; Gure-
 51 vich et al., 1992). The bursts last between ten and a few hundred microseconds (Marisaldi
 52 et al., 2014; Østgaard, Neubert, et al., 2019) with detected photon energies up to 40 MeV
 53 (Marisaldi et al., 2019). To explain the observed photon fluxes, one model considers am-
 54 plification of the electron flux in impulsive, 10-100 meter-scale, intense electric fields at
 55 the tip of lightning leaders (Moss et al., 2006; Celestin & Pasko, 2011; Xu et al., 2012;
 56 da Silva & Pasko, 2013; Chanrion et al., 2014; Köhn et al., 2017). In this scenario, TGFs
 57 would always be associated with optical radiation from leaders. In another model, the
 58 electron flux is created by the kilometer-scale electric fields within the clouds via backscat-
 59 tered X-rays and inversely propagating positrons, created by pair production to seed ad-
 60 dditional avalanches. This feedback mechanism suggests the TGF production to be as-
 61 sociated with modest levels of optical emissions if it is acting alone (Dwyer, 2008). Leader
 62 fields can help reaching the field threshold for the feedback mechanism.

63 Recent observations have shown that TGFs occur at the onset of optical emissions,
 64 which point to the importance of the lightning leader process (Neubert et al., 2020; Østgaard,
 65 Neubert, et al., 2019). The measurements were by the Atmosphere-Space Interactions
 66 Monitor (ASIM) on the International Space Station (ISS) that carries sensors in selected
 67 bands in the range from the infra-red to gamma-ray energies. With sensors on a com-
 68 mon platform, ambiguities in the relative timing of the sensor data are reduced, a prob-
 69 lem that has followed past studies attempting to correlate data from different satellites
 70 or on the ground (Østgaard et al., 2013; Gjesteland et al., 2017; Alnussirat et al., 2019).

71 In the study presented here, we analyze the UV and optical emissions detected by
 72 ASIM in connection with TGFs observed in the period from June 2018 to October 2019.
 73 We characterize the emissions relative to the TGF onset time, relate them to lightning
 74 propagation scenarios, and estimate their depth within the clouds. Section 2 gives an
 75 overview of the ASIM instruments, the data and the analysis methods; Section 3 presents
 76 the results and Section 4 a discussion.

77 2 Measurements and Analysis

78 ASIM on the ISS is designed to observe lightning, TGFs and Transient Luminous
 79 Events (TLEs) (Neubert et al., 2019). The instruments include the Modular Multi-spectral
 80 Imaging Array (MMIA) and the Modular X- and Gamma-ray Sensor (MXGS), both pointing
 81 towards nadir. The MXGS has a high-energy detector (\sim 0.3 to >30 MeV) that measures
 82 day and night with a time resolution of 28.7 ns and a low-energy detector (\sim 50-
 83 400 keV) that measures with a time resolution of 1 μ s, but only during the night because
 84 of optical photon contamination (Østgaard, Balling, et al., 2019). The MMIA includes
 85 three photometers and two cameras with the same field of view. The photometers sample
 86 at 100 kHz at 180-230 nm (UV), which includes part of the N₂ Lyman-Birge-Hopfield
 87 lines, at 337/4 nm (blue) (center of band/bandwidth) that includes the strongest line
 88 of N₂P, and at 777.4/5 nm (red), an OI line considered one of the strongest emission
 89 lines of the lightning spectrum. The cameras capture 12 frames per second at 337/4 nm
 90 and 777.4/3 nm with \sim 400x400 m ground resolution at nadir (Chanrion et al., 2019).
 91 MMIA is only operational during night to prevent damage by sunlight. The instrument
 92 computers include flash trigger logic that saves all sensor data if one sensor detects a flash.

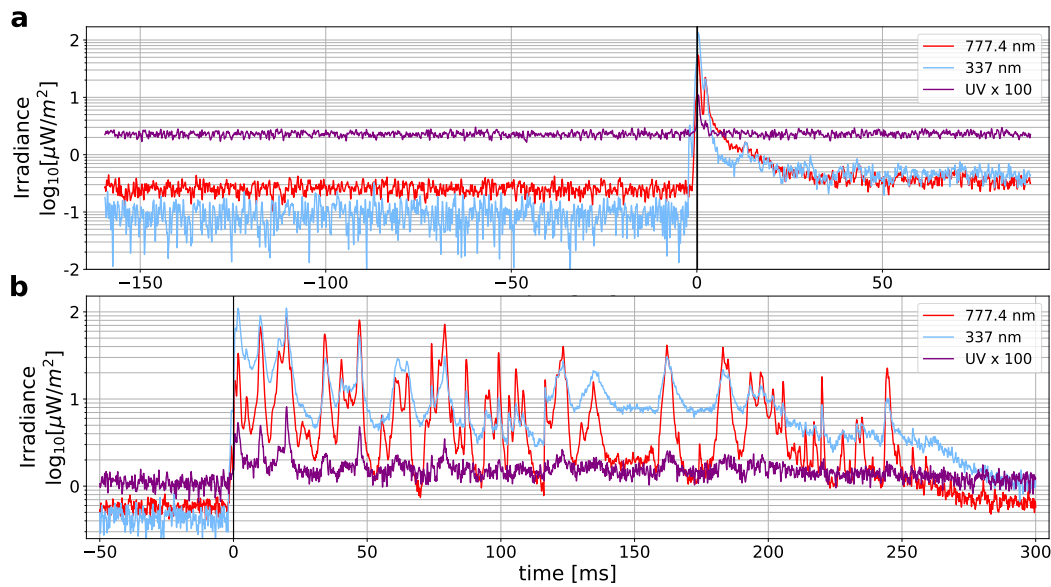


Figure 1. Typical optical signals observed in relation to TGFs. Time is relative to the detection of the first TGF photon on 26 May 2019, 02:29:34.993 (a) and 28 July 2018, 17:03:15.848 (b).

93 In the period extending from the end of the commissioning phase on 2 June 2018
 94 to 26 October 2019, ASIM observed 69 TGFs during the night inside the field of view
 95 (FOV) of the MMIA, all associated with optical emissions. The selected events were
 96 not associated with activity outside the MMIA FOV but inside the larger FOV of the
 97 Lightning Imaging Sensor on the ISS (ISS-LIS), rectangular with a diagonal of 1000 km
 98 (Blakeslee, 2019; Blakeslee et al., 2020), or the GLD360 network in a box of $\pm 6^\circ$ lati-
 99 tude and longitude; both within a 200 ms window centered at the TGF time. The like-
 100 lihood that the TGF events are associated with lightning activity not observed by the
 101 MMIA is then reduced. During the first ten months of nominal operation, the relative
 102 timing uncertainty between the MXGS and MMIA was up to $\pm 80 \mu\text{s}$, improving to ± 5
 103 μs after a software update in April 2019 (Østgaard, Neubert, et al., 2019). The absolute
 104 time accuracy is better than 25 ms, but can often be improved to ~ 1 ms by correlation
 105 with ground-based lightning detection data from, for instance, GLD360 and data from
 106 ISS-LIS. Such corrective improvement was possible for nearly 90% of the cases consid-
 107 ered here.

108 Two examples of the optical signals measured by the photometers are shown in Fig-
 109 ure 1. In both cases, the TGFs are preceded by lower level pre-activity and are followed
 110 by high amplitude emissions. In the less common case (Figure 1a), the TGFs are followed
 111 by few pulses, but more often they are followed by a longer sequence of pulses (Figure
 112 1b). In the analysis, we focus on a ± 20 ms time interval around the TGFs that includes
 113 the lower level activity prior to a TGF and the pulses that follow immediately after, but
 114 excludes continued, longer-duration activity after a TGF.

115 The optical signals are affected by photon scattering and absorption by cloud par-
 116 ticles, which determine the shape of the recorded light curve (Thomason & Krider, 1982;
 117 Koshak et al., 1994; Light et al., 2001). A convenient way to estimate scattering prop-
 118 erties is offered by Soler et al. (2020) and Luque et al. (2020). They present a model of
 119 an instantaneous, point-like source inside a planar, homogeneous cloud, where the nor-
 120 malized function describing the pulse shape observed above a cloud is:

$$121 f(t, t_0, \tau, \nu) = \sqrt{\frac{\tau}{\pi(t - t_0)^3}} \exp\left(2\sqrt{\nu\tau} - \frac{\tau}{t - t_0} - \nu(t - t_0)\right); \quad t > t_0 \quad (1)$$

122 where t is time, t_0 is the time when the source releases photons, τ is the charac-
 123 teristic diffusion time and ν is the absorption rate. For those TGF events that are as-

sociated with a simple optical pulse, we subtract the average background noise level, i.e. the radiance before the pre-activity in the interval [-150, -20] in Figure 1a before scaling and fitting the function to the pulse. The fitting procedure is illustrated in Figure 2 for the cases of modest pre-pulse activity (a) and high pre-pulse activity (b). Higher pre-pulse activity increases the uncertainties of the three fitting parameters, as discussed in a later section. We use the fitted function to define the times t_x where the pulses reach $x\%$ of their signal maximum and derive parameters such as the rise time, $t_{90} - t_{10}$, or the duration of full width at half maximum (FWHM), $t_{50t} - t_{50}$; t_{xt} denotes the times in the decaying tail of the pulse.

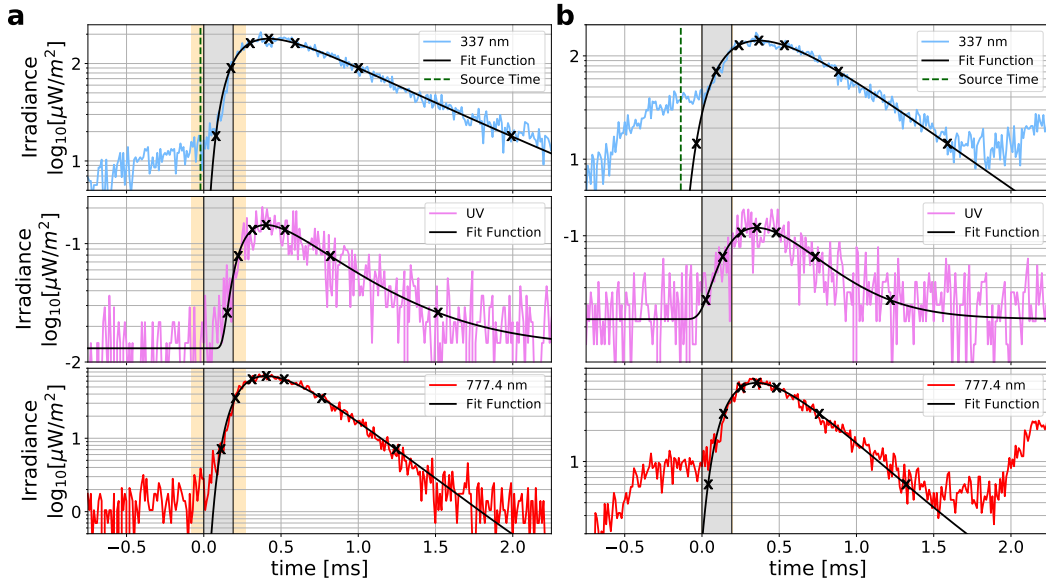


Figure 2. The functional fit to the photometer signals. **a)** Modest pre-pulse activity, **b)** high pre-pulse activity. A time of 0 ms is the start time of the TGF, the grey shaded region marks the duration of the TGF and the orange shaded region the respective time uncertainty of the measurement (± 80 and $\pm 5 \mu s$). The source time t_0 is indicated with a green, dashed line in the 337 nm band, crosses mark f_{10} , f_{50} , f_{90} , f_{max} , f_{90t} , f_{50t} , f_{10t} and thus the corresponding t_x and t_{xt} .

To estimate the physical nature of the cloud scattering that can be derived from the function, we chose the blue band and fit only the first half of the pulse to obtain new values for t_0 and τ . This wavelength is the least affected by absorption and the first half of the pulses is from photons that have undergone the least scattering in the cloud. They are therefore the least dependent on the model assumption of an horizontally infinite cloud.

138 A simulation model of photon scattering in arbitrary cloud geometries is described in
 139 Luque et al. (2020).

140 With τ , we can estimate the depth of the optical sources inside the clouds. There-
 141 fore, we need to make assumptions regarding size distribution and density of the cloud
 142 hydrometeors. These assumptions do not impact on the fitting of τ and get important
 143 solely in estimating the depths. The depth inside the cloud depends on τ and the dif-
 144 fusion coefficient, D , as $L = \sqrt{4D\tau}$. The diffusion coefficient is $D = \Lambda c/3(1 - g\omega_0)$
 145 where Λ is the mean free path of photons, c is the speed of light, g is a wavelength de-
 146 pendent asymmetry factor and ω_0 is the single scattering albedo. At 337 nm, $g \sim 0.88$
 147 and $\omega_0 \sim 1$. The mean free path depends on the size, r_c , and density, n_c , distributions
 148 of cloud particles as $\Lambda = 1/(2\pi r_c^2 n_c)$ (Thomason & Krider, 1982; Koshak et al., 1994;
 149 Light et al., 2001; Soler et al., 2020). Thus, we estimate L based on τ and the assump-
 150 tions for n_c , r_c , g and ω_0 .

151 3 Results

152 Of the 69 TGFs selected for analysis, 62 were followed by a strong optical pulse
 153 at 337 and 777.4 nm, which could be fitted with the function in Equation (1) in 52 cases.
 154 In the UV, 14 observations have pulses that could be fitted. We do not include three si-
 155 multaneous Elve detections, the luminous emissions in the ionosphere due to excitation
 156 by strong electromagnetic pulses from lightning, because of their different origin above
 157 the clouds (Neubert et al., 2020).

158 The results of the fits are summarized in Figure 3. The median source time t_0 is
 159 -10 ± 80 μ s relative to the first photon of the TGFs with outliers up to several ms (t_0 is
 160 only determined for the blue signal). The rise times are ~ 260 - 370 μ s and the FWHM
 161 is around 1 ms. The FWHM is somewhat larger for 337 nm than for 777.4 nm, consis-
 162 tent with more scattering of the blue photons and higher absorption of the red photons.
 163 Compared to statistics of lighting flashes without identified TGFs (Offroy et al., 2015;
 164 Christian & Goodman, 1987), the pulses presented here exhibit slightly longer rise times,
 165 $+50$ - 100 μ s, and doubled FWHMs, ~ 1 - 1.5 ms. The time parameters of UV emissions are
 166 more similar to the red than to the blue, but suffer generally most from atmospheric ab-
 167 sorption (Luque et al., 2020; Molina & Molina, 1986). Neither rise time nor FWHM are
 168 affected by the instrumental timing uncertainty. More values are given in the supplement.

169 The majority of the source times is within the instrumental and model uncertain-
 170 ties of the TGF start. We conclude, then, that the majority of optical pulses are emit-
 171 ted at the onset of TGFs, consistent with previous case studies (Neubert et al., 2020;
 172 Østgaard, Neubert, et al., 2019; Alnussirat et al., 2019), with some cases delayed up to
 173 ~4 ms. The uncertainties are discussed further in the next section. The optical source
 174 duration is modeled by a function that describes an instantaneous source, suggesting that
 175 the pulse duration may be caused by cloud scattering, just as TGF pulses are broadened
 176 by Compton scattering of the photons (Celestin & Pasko, 2012). Both sources, optical
 177 and gamma ray, are then likely of comparable duration.

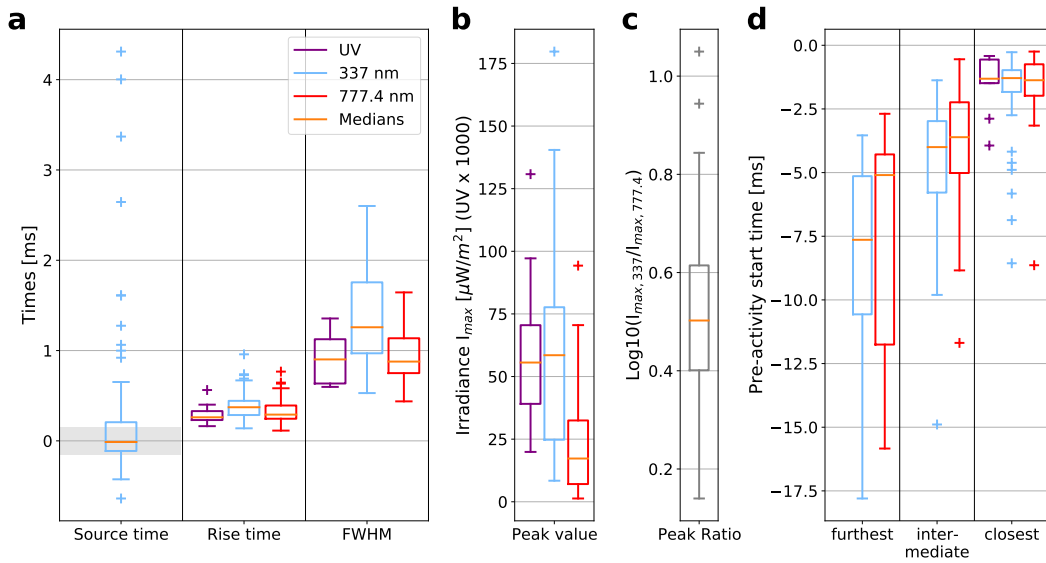


Figure 3. Characteristics of the optical peak following a TGF. The boxes represent the interquartile range of the values from the 25th to 75th percentile and the horizontal lines within are the median values. The whiskers extend to 1.5 times the interquartile range or to the maximum and minimum values if they are lower, outliers are shown as '+'. **a)** The temporal characteristics for each photometer band. From left to right they are the source time (t_0) relative to the arrival of the first TGF photon, the rise time and the FWHM. The grey shaded area in the interval [-0.15, 0.15] ms indicates the uncertainty as discussed later. **b)** Irradiance of the optical pulses in the three bands. The irradiance in the UV band is multiplied by 1000 to show it on the same scale as the other bands. **c)** Ratio of the peak values of 337 nm and 777 nm. **d)** start of the pre-activity pulses relative to start of the main pulse.

178 The peak irradiance in the blue is generally ~3 times stronger than in the red (Fig-
 179 ures 3b,c), while 777.4 nm emissions dominate regular lightning pulses, i.e. ratios ≤ 1 (e.g.

180 Adachi et al., 2016). For the cases with UV pulses, the amplitudes of the blue and the
181 UV correlate with a magnitude difference of 10^3 .

182 Close to 90% of the TGF observations had corresponding ISS-LIS or GLD360 de-
183 tections, matching in location inside the FOV and allowing us to correct the absolute
184 timing. We find GLD and LIS detections, when available, to be associated with the main
185 optical pulse, not the TGF itself. This has implications for studies that correlate TGF
186 events with ground observations of lightning.

187 During the pre-activity, the red and blue photometer signals increased when ap-
188 proaching the onset of the main optical pulse, with 1-3 smaller pulses in the signal am-
189 plitude. The majority of observations had two pulses while a third had three pulses. In
190 the UV band, 9 observations had one preceding pulse, more than one was not observed.
191 The statistics of pre-activity start times in Figure 3d is sorted by the temporal proxim-
192 ity of the pulses to the main optical pulse and shows the intervals between the pulses
193 shorten when approaching the main peak. Optical emissions more than 20 ms prior to
194 the TGF from the same location were observed in 2 of the 52 cases. In both of them,
195 the detections were of low intensity and dominantly blue, consistent with the the rest
196 of the pre-activity measurements. Consequently, TGFs occur in the initial phase of a flash
197 without extensive optical activity before them. Intensities and durations of the pre-activity
198 pulses can be found in the supplement.

199 The depth in the clouds of the optical sources at TGF onset were estimated from
200 the fit of the first half of the blue photometer signal, as described earlier. We assume a
201 cloud top composition of water ice droplets with typical values $r_c = 15, 20 \mu\text{m}$ and $n_c =$
202 $2.5 \cdot 10^8 \text{ m}^{-3}$ (Dye et al., 2007; Ursi et al., 2019) while also accounting for the direction
203 from the source to the detector relative to zenith. The altitude is estimated by assum-
204 ing the cloud tops are at the tropopause (Splitt et al., 2010; Ursi et al., 2019) and that
205 the tropopause altitude follows Equation (2) of Offroy et al. (2015).

206 The result is shown in Figure 4. The optical sources that can be approximated by
207 the fit function (75% of the events) are in the top of the cloud and at a few km depth,
208 consistent with Stanley et al. (2006); Cummer et al. (2015). The depth and altitude de-
209 pend on the parameters that enter the assumptions on the cloud particles, where less dense
210 clouds, $r_c = 15 \mu\text{m}$, lead to greater depths. For $n_c = 10^8 \text{ m}^{-3}$, the altitudes are 1-2
211 km lower.

212 We conclude this section by noting a simple method to estimate the parameter τ ,
 213 which is the only pulse parameter entering the altitude estimation. We find it can be ap-
 214 proximated from the FWHM as $\tau = k \cdot FWHM + d$ with $k = 0.853 \pm 0.29$ and $d =$
 215 -0.001 ± 0.429 , see also Figure S4 in the supplement.

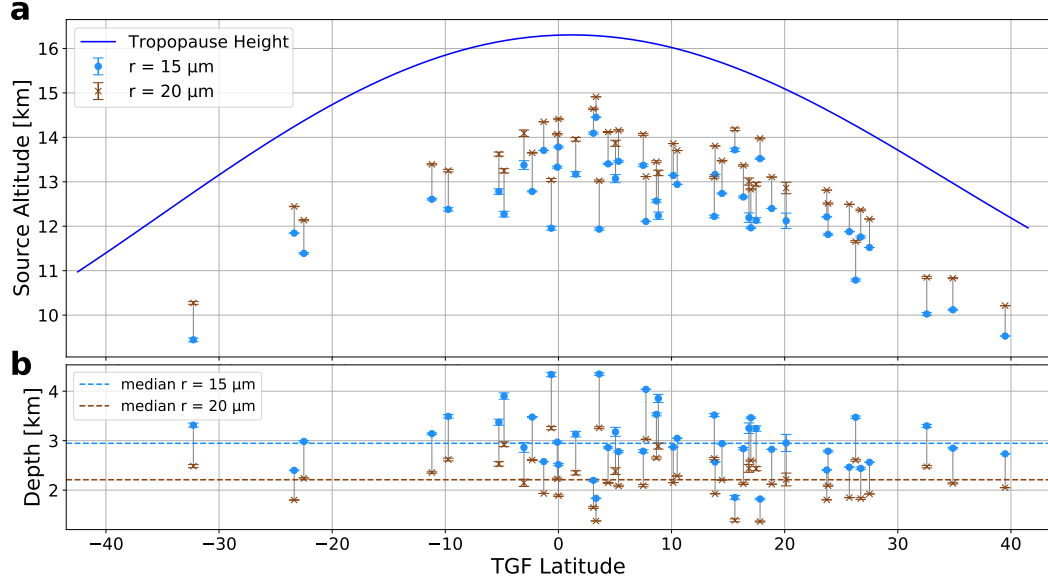


Figure 4. Estimated source altitudes (a) and depths inside clouds (b) of the optical pulses associated with TGFs for $n_c = 2.5 \cdot 10^8 \text{ m}^{-3}$.

216 4 Discussion and Interpretation

217 Upward negative intra-cloud leaders in the upper cloud regions are thought to prop-
 218 agate from the central negative charge region towards the upper positive charge region
 219 while producing 1-3 bursts of initial breakdown pulses (IBPs) with 1-5 ms between the
 220 bursts. IBPs are signatures in signals measured by electric field sensors (Marshall et al.,
 221 2013). Video recordings from the ground show luminosity increases in the visible spec-
 222 trum at the time of large IBPs (Stolzenburg et al., 2016). The observation of 1-3 pre-
 223 activity pulses with increasing intensity observed by ASIM agrees then well with upward
 224 propagating leaders that produce luminous IBP bursts (cf. supplementary Figure S2).
 225 Shorter intervals of the pulses (Figure 3d) further suggest an upward acceleration of the
 226 leaders as discussed in Cummer et al. (2015).

227 The characteristics of the main optical pulses associated with the TGFs appear con-
 228 sistent with the so-called energetic in-cloud pulses (EIPs) observed by ground networks

in LF signals (30-300 kHz). EIPs are typically detected within a few ms after the initiation of upward negative leaders in the upper regions of the clouds (Lyu et al., 2015, 2016), as also seen in Figure 4. Whereas Lyu et al. (2018) find that at least some TGFs are associated with large currents, we find that all TGFs have associated red pulses, indicating significant leader current flow (e.g. Bitzer et al., 2016). The red signal is atypically weaker than the blue and both bands show twice as long pulse durations (FWHM) compared to normal lightning pulses without identified TGFs (Offroy et al., 2015; Christian & Goodman, 1987; Adachi et al., 2016). The similarity of the main pulse and EIP characteristics suggests the pulses to be the optical equivalent of EIPs.

The optical scattering properties of the cloud, estimated from the fit function, must be taken with caution since lightning is spatially and temporally extended. However, as long as the source onset is short compared to the rise times of the optical pulses, i.e. less than $\sim 100 \mu\text{s}$, we find the fit function to the first half of the pulse, from which we estimate t_0 and τ , to be relatively insensitive to the assumption on the temporal variation of the source. Nevertheless, the source duration is likely much shorter than the measured pulse durations and likely in the range of TGF sources, which are typically a few $100 \mu\text{s}$ or less (Marisaldi et al., 2014; Østgaard, Neubert, et al., 2019). As in scattering of optical emissions, TGFs are broadened by Compton scattering (Celestin & Pasko, 2012), indicating that the sources are a few tens of μs in duration. The average duration of EIPs in LF waveforms is $55 \mu\text{s}$ (Lyu et al., 2015). Consequently, all inferred source durations related to TGF detection (LF, optical, TGF photons) are down to ~ 10 to few $100 \mu\text{s}$.

To investigate the accuracy of t_0 , we derived t_0 from the red signal (leader emissions) and compared it to the start times of UV signatures of two cases with simultaneous Elves (powered by electromagnetic pulses from impulsive leader currents). We find $t_{0,\text{red}}$ to be 59 ± 8 and $22 \pm 7 \mu\text{s}$ before the onset of the Elve emissions in the UV, while $t_{0,\text{blue}}$ was 113 ± 6 and $99 \pm 8 \mu\text{s}$ earlier. Since Elve emissions are unaffected by cloud scattering, they are an estimate of the onset time of the current pulses. Elves are expanding rings in the lower ionosphere extending several 100 km in horizontal radius. The detection of their onset is typically $\sim 20 \mu\text{s}$ delayed due to the geometry of the emissions relative to the sensors. Accounting for this delay, $t_{0,\text{red}}$ is ~ 40 and $\sim 0 \mu\text{s}$ before the Elve. However, this example also shows how the pre-activity interferes with the fitting procedure on this precise level: The Elve case with a 777-UV delay of $22/\sim 0 \mu\text{s}$ has a pre-activity intensity of $< 5\%$, while the maximum pre-activity intensity was $\sim 30\%$ in the case with

the larger delay ($\sim 60/40 \mu\text{s}$). Therefore, we have to assume that pre-activity levels above $\sim 20\%$ of the main pulse intensity introduce methodical uncertainties of up to $\sim 30\text{-}40 \mu\text{s}$, valid also for the blue activity and the respective t_0 values. Additional uncertainty is possibly introduced by Elve emissions in the blue band. From the cases studied, we expect intensities less than those in the UV, $\sim 3\text{-}4 \mu\text{W}/\text{m}^2$, which are of the order of, or smaller than, the pre-activity. The analysis of the two Elves indicates the mutual production of the red leader emissions and the Elves, while the blue emissions appear to start before this phase.

With the instrumental and methodical uncertainties, ± 80 or $\pm 5 \mu\text{s}$ as mentioned earlier and $\sim 30\text{-}40 \mu\text{s}$ respectively, the median source time of the optical pulses at $-10 \mu\text{s}$ before the TGF onset (Figure 3a) is smaller than the accuracy of the source time identification and does not allow to address the sequence of the events. For outliers more than $\sim 150 \mu\text{s}$ before or after the TGF onset, the sequence seems to be clear, provided we have identified the correct pulse associations with the TGF.

The consistent occurrence of optical signals in the blue and red bands for all TGFs connects TGF production to streamer and leader processes. Optical detections after the main peak, observed for some events (Figure 1b), is likely continued leader activity and branching in the cloud (Cummer et al., 2015). In our understanding, dominating blue emissions in the main pulses (Figure 3b,c) indicate high levels of streamer activity. Combined with measurements of VHF (30-300 MHz) activity related to TGFs by others, proposed to be a signature of temporally and spatially extended source regions (Lyu et al., 2018), we suggest a scenario where the optical and TGF emissions are generated as the atmosphere of the region ahead of the leader tip breaks down in a flash of streamers, high-energy electrons and a leader current surge.

286 Acknowledgments

MH appreciates discussions with and feedback from Joe Dwyer. We thank VAISALA for the GLD360 lightning data. **Funding:** ASIM is a mission of the European Space Agency (ESA) and is funded by ESA and by national grants of Denmark, Norway and Spain. The ASIM Science Data Centre is supported by ESA PRODEX contracts C 4000115884 (DTU) and 4000123438 (Bergen). The science analysis is supported by: the European Research Council grant n. 320839, the Research Council of Norway contracts 223252/F50 (CoE/BCSS), the Ministerio Ciencia e Innovacion grant ESP 2017- 86263-C4, and project

grant PID2019-109269RB. This project has received funding from the European Union's Horizon 2020 research and innovation programme under the Marie Skłodowska-Curie grant agreement 722337. **Competing interests:** The authors declare no competing interests. **Data and materials availability:** ASIM data and Vaisala GLD360 detections are available via asdc.space.dtu.dk. ISS-LIS data is available from (Blakeslee, 2019)

299 References

- 300 Adachi, T., Sato, M., Ushio, T., Yamazaki, A., Suzuki, M., Kikuchi, M., ...
 301 Kusunoki, K. (2016, jul). Identifying the occurrence of lightning and
 302 transient luminous events by nadir spectrophotometric observation. *Journal*
 303 *of Atmospheric and Solar-Terrestrial Physics*, 145, 85–97. Retrieved
 304 from <http://dx.doi.org/10.1016/j.jastp.2016.04.010> https://
 305 linkinghub.elsevier.com/retrieve/pii/S1364682616301109 doi:
 306 10.1016/j.jastp.2016.04.010
- 307 Alnussirat, S. T., Christian, H. J., Fishman, G. J., Burchfield, J., & Cherry, M. L.
 308 (2019, oct). Simultaneous space-based observations of terrestrial gamma-
 309 ray flashes and lightning optical emissions: Investigation of the terrestrial
 310 gamma-ray flash production mechanisms. *Physical Review D*, 100(8),
 311 083018 1–7. Retrieved from [https://doi.org/10.1103/PhysRevD.100](https://doi.org/10.1103/PhysRevD.100.083018)
 312 .083018 https://link.aps.org/doi/10.1103/PhysRevD.100.083018 doi:
 313 10.1103/PhysRevD.100.083018
- 314 Bitzer, P. M., Burchfield, J. C., & Christian, H. J. (2016, mar). A Bayesian Ap-
 315 proach to Assess the Performance of Lightning Detection Systems. *Journal*
 316 *of Atmospheric and Oceanic Technology*, 33(3), 563–578. Retrieved from
 317 <http://journals.ametsoc.org/doi/10.1175/JTECH-D-15-0032.1> doi:
 318 10.1175/JTECH-D-15-0032.1
- 319 Blakeslee, R. J. (2019). *Non-Quality Controlled Lightning Imaging Sensor (LIS)*
 320 *on International Space Station (ISS) Science Data*. NASA Global Hydrology
 321 Resource Center DAAC, Huntsville, Alabama, U.S.A. Retrieved from http://https://ghrc.nsstc.nasa.gov/hydro/details/isslis.v1_nqc doi: <http://dx.doi.org/10.5067/LIS/ISSLIS/DATA107>
- 324 Blakeslee, R. J., Lang, T. J., Koshak, W. J., Buechler, D., Gatlin, P., Mach, D. M.,
 325 ... Christian, H. (2020, jul). Three years of the Lightning Imaging Sensor

- 326 onboard the International Space Station: Expanded Global Coverage and
 327 Enhanced Applications. *Journal of Geophysical Research: Atmospheres*, 1–
 328 20. Retrieved from <https://onlinelibrary.wiley.com/doi/abs/10.1029/2020JD032918> doi: 10.1029/2020JD032918
- 330 Celestin, S., & Pasko, V. P. (2011, mar). Energy and fluxes of thermal runaway
 331 electrons produced by exponential growth of streamers during the stepping
 332 of lightning leaders and in transient luminous events. *Journal of Geophysical Research: Space Physics*, 116(A03315), 1–14. Retrieved from <http://doi.wiley.com/10.1029/2010JA016260> doi: 10.1029/2010JA016260
- 333 Celestin, S., & Pasko, V. P. (2012, jan). Compton scattering effects on the dura-
 334 tion of terrestrial gamma-ray flashes. *Geophysical Research Letters*, 39(2). Re-
 335 tried from <http://doi.wiley.com/10.1029/2011GL050342> doi: 10.1029/2011GL050342
- 336 Chanrion, O., Bonaventura, Z., Çinar, D., Bourdon, A., & Neubert, T. (2014,
 337 may). Runaway electrons from a beam-bulk' model of streamer: application
 338 to TGFs. *Environmental Research Letters*, 9(5), 055003. Retrieved from
<https://iopscience.iop.org/article/10.1088/1748-9326/9/5/055003>
 339 doi: 10.1088/1748-9326/9/5/055003
- 340 Chanrion, O., Neubert, T., Lundgaard Rasmussen, I., Stoltze, C., Tcherniak, D.,
 341 Jessen, N. C., ... Lorenzen, M. (2019, jun). The Modular Multispectral
 342 Imaging Array (MMIA) of the ASIM Payload on the International Space
 343 Station. *Space Science Reviews*, 215(4), 28. Retrieved from <http://dx.doi.org/10.1007/s11214-019-0593-y>
 344 doi: 10.1007/s11214-019-0593-y
- 345 Christian, H. J., & Goodman, S. J. (1987, dec). Optical Observations of Lightning
 346 from a High-Altitude Airplane. *Journal of Atmospheric and Oceanic Technol-
 347 ogy*, 4(4), 701–711. Retrieved from <http://journals.ametsoc.org/doi/abs/10.1175/1520-0426%281987%29004%3C0701%3A000OLFA%3E2.0.CO%3B2> doi: 10
 348 .1175/1520-0426(1987)004<701:OOOLFA>2.0.CO;2
- 349 Cummer, S. A., Lyu, F., Briggs, M. S., Fitzpatrick, G., Roberts, O. J., & Dwyer,
 350 J. R. (2015). Lightning leader altitude progression in terrestrial gamma-
 351 ray flashes. *Geophysical Research Letters*, 42(18), 7792–7798. doi:
 352 10.1002/2015GL065228

- 359 da Silva, C. L., & Pasko, V. P. (2013, dec). Dynamics of streamer-to-leader transi-
360 tion at reduced air densities and its implications for propagation of lightning
361 leaders and gigantic jets. *Journal of Geophysical Research: Atmospheres*,
362 118(24), 13,561–13,590. Retrieved from <http://doi.wiley.com/10.1002/2013JD020618> doi: 10.1002/2013JD020618
- 364 Dwyer, J. R. (2008, may). Source mechanisms of terrestrial gamma-ray flashes.
365 *Journal of Geophysical Research*, 113(D10), D10103. Retrieved from <http://doi.wiley.com/10.1029/2007JD009248> doi: 10.1029/2007JD009248
- 366 Dye, J. E., Bateman, M. G., Christian, H. J., Defer, E., Grainger, C. A., Hall,
368 W. D., ... Willis, P. T. (2007, jun). Electric fields, cloud microphysics,
369 and reflectivity in anvils of Florida thunderstorms. *Journal of Geophysical Re-
370 search*, 112(D11), D11215. Retrieved from <http://doi.wiley.com/10.1029/2006JD007550> doi: 10.1029/2006JD007550
- 372 Fishman, G. J., Bhat, P. N., Mallozzi, R., Horack, J. M., Koshut, T., Kouveliotou,
373 C., ... Goodman, S. J. (1994). Discovery of Intense Gamma-Ray Flashes of
374 Atmospheric Origin. *Science*, 264(5163), 1313–1316.
- 375 Gjesteland, T., Østgaard, N., Bitzer, P., & Christian, H. J. (2017, jul). On the
376 timing between terrestrial gamma ray flashes, radio atmospherics, and optical
377 lightning emission. *Journal of Geophysical Research: Space Physics*, 122(7),
378 7734–7741. Retrieved from <http://doi.wiley.com/10.1002/2017JA024285>
379 doi: 10.1002/2017JA024285
- 380 Gurevich, A., Milikh, G., & Roussel-Dupre, R. (1992, jun). Runaway electron mech-
381 anism of air breakdown and preconditioning during a thunderstorm. *Physics
382 Letters A*, 165(5-6), 463–468. Retrieved from <https://linkinghub.elsevier.com/retrieve/pii/037596019290348P> doi: 10.1016/0375-9601(92)90348-P
- 384 Köhn, C., Diniz, G., & Harakeh, M. N. (2017). Production mechanisms of
385 leptons, photons, and hadrons and their possible feedback close to light-
386 ning leaders. *Journal of Geophysical Research*, 122(2), 1365–1383. doi:
387 10.1002/2016JD025445
- 388 Koshak, W. J., Solakiewicz, R. J., Phanord, D. D., & Blakeslee, R. J. (1994). Dif-
389 fusion model for lightning radiative transfer. *Journal of Geophysical Research*,
390 99(D7), 14361–14371.
- 391 Light, T. E., Suszcynsky, D. M., Kirkland, M. W., & Jacobson, A. R. (2001,

- 392 aug). Simulations of lightning optical waveforms as seen through clouds by
393 satellites. *Journal of Geophysical Research: Atmospheres*, 106(D15), 17103–
394 17114. Retrieved from <http://doi.wiley.com/10.1029/2001JD900051> doi:
395 10.1029/2001JD900051
- 396 Luque, A., Gordillo-Vázquez, F. J., Li, D., Malagón-romero, A., Pérez-invernón,
397 F. J., Schmalzried, A., ... Østgaard, N. (2020). Modeling lightning obser-
398 vations from space-based platforms (CloudScat.jl 1.0). *Geoscientific Model*
399 *Development Discussion*. doi: 10.5194/gmd-2020-161
- 400 Lyu, F., Cummer, S. A., Briggs, M., Marisaldi, M., Blakeslee, R. J., Bruning, E.,
401 ... Stanbro, M. (2016, aug). Ground detection of terrestrial gamma ray
402 flashes from distant radio signals. *Geophysical Research Letters*, 43(16), 8728–
403 8734. Retrieved from <http://doi.wiley.com/10.1002/2016GL070154> doi:
404 10.1002/2016GL070154
- 405 Lyu, F., Cummer, S. A., Krehbiel, P. R., Rison, W., Briggs, M. S., Cramer, E., ...
406 Stanbro, M. (2018, feb). Very High Frequency Radio Emissions Associated
407 With the Production of Terrestrial Gamma-Ray Flashes. *Geophysical Research*
408 *Letters*, 45(4), 2097–2105. Retrieved from <http://doi.wiley.com/10.1002/2018GL077102> doi: 10.1002/2018GL077102
- 410 Lyu, F., Cummer, S. A., & McTague, L. (2015, aug). Insights into high peak cur-
411 rent incloud lightning events during thunderstorms. *Geophysical Research Let-
412 ters*, 42(16), 6836–6843. Retrieved from <https://onlinelibrary.wiley.com/doi/abs/10.1002/2015GL065047> doi: 10.1002/2015GL065047
- 414 Marisaldi, M., Fuschino, F., Tavani, M., Dietrich, S., Price, C., Galli, M., ... Ver-
415 cellone, S. (2014, feb). Properties of terrestrial gamma ray flashes detected
416 by AGILE MCAL below 30 MeV. *Journal of Geophysical Research: Space*
417 *Physics*, 119(2), 1337–1355. Retrieved from <http://doi.wiley.com/10.1002/2013JA019301> doi: 10.1002/2013JA019301
- 419 Marisaldi, M., Galli, M., Labanti, C., Østgaard, N., Sarria, D., Cummer, S. A.,
420 ... Verrecchia, F. (2019, jul). On the HighEnergy Spectral Component
421 and Fine Time Structure of Terrestrial Gamma Ray Flashes. *Journal of*
422 *Geophysical Research: Atmospheres*, 124(14), 7484–7497. Retrieved from
423 <https://onlinelibrary.wiley.com/doi/abs/10.1029/2019JD030554> doi:
424 10.1029/2019JD030554

- 425 Marshall, T., Stolzenburg, M., Karunaratne, S., Cummer, S., Lu, G., Betz, H.-D.,
 426 ... Xiong, S. (2013, oct). Initial breakdown pulses in intracloud lightning
 427 flashes and their relation to terrestrial gamma ray flashes. *Journal of Geo-*
 428 *physical Research: Atmospheres*, 118(19), 10,907–10,925. Retrieved from
 429 <http://doi.wiley.com/10.1002/jgrd.50866> doi: 10.1002/jgrd.50866
- 430 Molina, L. T., & Molina, M. J. (1986). Absolute absorption cross sections of
 431 ozone in the 185- to 350-nm wavelength range. *Journal of Geophysical Re-*
 432 *search*, 91(D13), 14501. Retrieved from <http://doi.wiley.com/10.1029/JD091iD13p14501> doi: 10.1029/JD091iD13p14501
- 433 Moss, G. D., Pasko, V. P., Liu, N., & Veronis, G. (2006). Monte Carlo model for
 434 analysis of thermal runaway electrons in streamer tips in transient luminous
 435 events and streamer zones of lightning leaders. *Journal of Geophysical Re-*
 436 *search*, 111(A2), A02307. Retrieved from <http://doi.wiley.com/10.1029/2005JA011350> doi: 10.1029/2005JA011350
- 437 Neubert, T., Østgaard, N., Reglero, V., Blanc, E., Chanrion, O., Oxborow, C. A.,
 438 ... Bhanderi, D. D. V. (2019, mar). The ASIM Mission on the Interna-
 439 tional Space Station. *Space Science Reviews*, 215(2), 26. Retrieved from
 440 <http://dx.doi.org/10.1007/s11214-019-0592-z> <http://link.springer.com/10.1007/s11214-019-0592-z> doi: 10.1007/s11214-019-0592-z
- 441 Neubert, T., Østgaard, N., Reglero, V., Chanrion, O., Heumesser, M., Dimitriadou,
 442 K., ... Eyles, C. J. (2020, dec). A terrestrial gamma-ray flash and ionospheric
 443 ultraviolet emissions powered by lightning. *Science*, 367(6474), 183–186.
 444 Retrieved from <https://science.sciencemag.org/content/367/6474/183>
 445 <https://www.sciencemag.org/lookup/doi/10.1126/science.aax3872>
 446 doi: 10.1126/science.aax3872
- 447 Offroy, M., Farges, T., Kuo, C. L., Chen, A. B. C., Hsu, R. R., Su, H. T., ... Frey,
 448 H. U. (2015, aug). Temporal and radiometric statistics on lightning flashes
 449 observed from space with the ISUAL spectrophotometer. *Journal of Geophys-*
 450 *ical Research*, 120(15), 7586–7598. Retrieved from <http://doi.wiley.com/10.1002/2015JD023263> doi: 10.1002/2015JD023263
- 451 Østgaard, N., Balling, J. E., Bjørnseth, T., Brauer, P., Budtz-Jørgensen, C., Bujwan,
 452 W., ... Yang, S. (2019). The Modular X- and Gamma-Ray Sensor (MXGS)
 453 of the ASIM Payload on the International Space Station. *Space Science Re-*

- 458 *views*, 215(2), 23. Retrieved from <http://link.springer.com/10.1007/s11214-018-0573-7>
459
460 Østgaard, N., Gjesteland, T., Carlson, B. E., Collier, A. B., Cummer, S. A., Lu,
461 G., & Christian, H. J. (2013, may). Simultaneous observations of optical
462 lightning and terrestrial gamma ray flash from space. *Geophysical Research
463 Letters*, 40(10), 2423–2426. Retrieved from <http://doi.wiley.com/10.1002/grl.50466> doi: 10.1002/grl.50466
464
465 Østgaard, N., Neubert, T., Reglero, V., Ullaland, K., Yang, S., Genov, G., ... Al-
466 nussirat, S. (2019, dec). First 10 Months of TGF Observations by ASIM.
467 *Journal of Geophysical Research: Atmospheres*, 124, 2019JD031214. Retrieved
468 from <https://onlinelibrary.wiley.com/doi/abs/10.1029/2019JD031214>
469 doi: 10.1029/2019JD031214
470
471 Soler, S., PérezInvernón, F. J., GordilloVázquez, F. J., Luque, A., Li, D.,
472 MalagónRomero, A., ... Østgaard, N. (2020, jul). Blue optical observa-
473 tions of narrow bipolar events by ASIM suggest corona streamer activity in
474 thunderstorms. *Journal of Geophysical Research: Atmospheres*. Retrieved from
475 <https://onlinelibrary.wiley.com/doi/abs/10.1029/2020JD032708> doi:
476 10.1029/2020JD032708
477
478 Splitt, M. E., Lazarus, S. M., Barnes, D., Dwyer, J. R., Rassoul, H. K., Smith,
479 D. M., ... Grefenstette, B. (2010, jun). Thunderstorm characteristics as-
480 sociated with RHESSI identified terrestrial gamma ray flashes. *Journal of
481 Geophysical Research: Space Physics*, 115(A6). Retrieved from <http://doi.wiley.com/10.1029/2009JA014622> doi: 10.1029/2009JA014622
482
483 Stanley, M. A., Shao, X.-M., Smith, D. M., Lopez, L. I., Pongratz, M. B., Harlin,
484 J. D., ... Regan, A. (2006). A link between terrestrial gamma-ray flashes
485 and intracloud lightning discharges. *Geophysical Research Letters*, 33(6),
486 L06803. Retrieved from <http://doi.wiley.com/10.1029/2005GL025537> doi:
487 10.1029/2005GL025537
488
489 Stolzenburg, M., Marshall, T. C., Karunaratne, S., & Orville, R. E. (2016, sep).
490 Luminosity with intracloud-type lightning initial breakdown pulses and ter-
restrial gamma-ray flash candidates. *Journal of Geophysical Research: At-
mospheres*, 121(18), 10,919–10,936. Retrieved from <http://doi.wiley.com/10.1002/2016JD025202> doi: 10.1002/2016JD025202

- 491 Thomason, L. W., & Krider, E. P. (1982, sep). The Effects of Clouds on the
492 Light Produced by Lightning. *Journal of the Atmospheric Sciences*, 39(9),
493 2051–2065. Retrieved from <http://journals.ametsoc.org/doi/abs/10.1175/1520-0469%281982%29039%3C2051%3ATEOCOT%3E2.0.CO%3B2> doi:
494 10.1175/1520-0469(1982)039(2051:TEOCOT)2.0.CO;2
495 Ursi, A., Marisaldi, M., Dietrich, S., Tavani, M., Tiberia, A., & Porcù, F. (2019,
496 dec). Analysis of Thunderstorms Producing Terrestrial Gamma Ray
497 Flashes With the Meteosat Second Generation. *Journal of Geophys-
498 ical Research: Atmospheres*, 124(23), 12667–12682. Retrieved from
499 <https://onlinelibrary.wiley.com/doi/abs/10.1029/2018JD030149> doi:
500 10.1029/2018JD030149
501 Wilson, C. T. R. (1925). The electric field of a thunderstorm and some of its effects.
502 *Proceedings of the Royal Society of London*, 37(32D), 32D–37D. doi: 10.1088/
503 1478-7814/37/1/314
504 Xu, W., Celestin, S., & Pasko, V. P. (2012, apr). Source altitudes of terrestrial
505 gamma-ray flashes produced by lightning leaders. *Geophysical Research Let-
506 ters*, 39(8). Retrieved from <http://doi.wiley.com/10.1029/2012GL051351>
507 doi: 10.1029/2012GL051351